Biomechanics of actin filaments: a computational multi-level study

Biomechanics of actin filaments: A computational multi-level study

Marco A. Deriu [a,*], Tamara C. Bidone [a], Francesco Mastrangelo [a], Giacomo Di Benedetto [a], Monica Soncini [b], Franco M. Montevecchi [a], Umberto Morbiducci [a]

[a] Department of Mechanics, Politecnico di Torino, Italy
[b] Department of Bioengineering, Politecnico di Milano, Italy

A B S T R A C T

The actin microfilament (F-actin) is a structural and functional component of the cell cytoskeleton. Notwithstanding the primary role it plays for the mechanics of the cell, the mechanical behaviour of F-actin is still not totally explored. In particular, the relationship between the mechanics of F-actin and its molecular architecture is not completely understood.

In this study, the mechanical properties of F-actin were related to the molecular topology of its building monomers (G-actin) by employing a computational multi-level approach. F-actins with lengths up to 500 nm were modelled and characterized, using a combination of equilibrium molecular dynamics (MD) simulations and normal mode analysis (NMA). MD simulations were performed to analyze the molecular rearrangements of G-actin in physiological conditions; NMA was applied to compute the macroscopic properties of F-actin from its vibrational modes of motion.

Results from this multi-level approach showed that bending stiffness, bending modulus and persistence length are independent from the length of F-actin. On the contrary, the orientations and motions of selected groups of residues of G-actin play a primary role in determining the filament flexibility.

In conclusion, this study (i) demonstrated that a combined computational approach of MD and NMA allows to investigate the biomechanics of F-actin taking into account the molecular topology of the filament (i.e., the molecular conformations of G-actin) and (ii) that this can be done using only crystallographic G-actin, without the need of introducing experimental parameters nor of reducing the number of residues.

1. Introduction

Actin, the most abundant cytoskeleton protein, can be found in globular (G-actin) and filamentous (F-actin) forms. G-actin consists of four functional subdomains (Fig. 1a) that rearrange upon polymerization into F-actin. F-actin is the functional form of the protein (Pollard et al., 2000) and it is involved in many cellular processes, as muscle contraction, cell motility, cell division, vesicle and organelle movement, cell signaling, maintenance of cell junctions and cell shape (Gittes et al., 1993; Gov et al., 2006; Howard, 2001; Isambert et al., 1995; Jeon et al., 2008; Kojima et al., 1994; McCullough et al., 2008; Otterbein et al., 2001; Stricker et al., 2010; Tsuda et al., 1996; Yang et al., 2008).

F-actin performs structural and functional activities (Kabsch and Vandekerckhove, 1992; Pfaendtner et al., 2010). For this reason, F-actin must ensure adequate mechanical properties, such as sufficient resistance to bending. Moreover, also the dynamic properties of F-actin, as those modulating the action of molecular motors, are directly related to the filament elasticity (Chu et al., 2006). The basis of the mechanical behaviour of F-actin relies on both the molecular structure of G-actins and on the intermolecular interactions holding monomers together into a hierarchical arrangement (McCullough et al., 2008). Several studies have been carried out in order to measure mechanical properties of F-actin (Table 1).

In particular, it has been found that: (i) the persistence length, a measure of the filament propensity to fluctuate under thermal motion (Gardel et al., 2003) ranges from about 1 μm (Chu and Voth, 2006; Lyman et al., 2008; Scharf and Newman, 1995), to nearly 10–15 μm (Cameron et al., 2001; Janmey et al., 1994; Liu and Pollack, 2002), up to roughly 20 μm (Gittes et al., 1993; Isambert et al., 1995; Ott et al., 1993); (ii) the flexural rigidity ranges from 1.9×10^{-26} Nm^2 (Fujime and Ishiwata, 1971), to 6.6×10^{-26} Nm^2 (Yasuda et al., 1996) and 7.3×10^{-26} Nm^2 (Gittes et al., 1993), up to about 12.6×10^{-26} Nm^2 (Panke et al., 2001); and (iii) the Young modulus ranges from 1.8 GPa (Kojima et al., 1994) to about 2.6 GPa (Gittes et al., 1993).

Previous computational studies investigated molecular features and mechanisms responsible for F-actin mechanics by making a

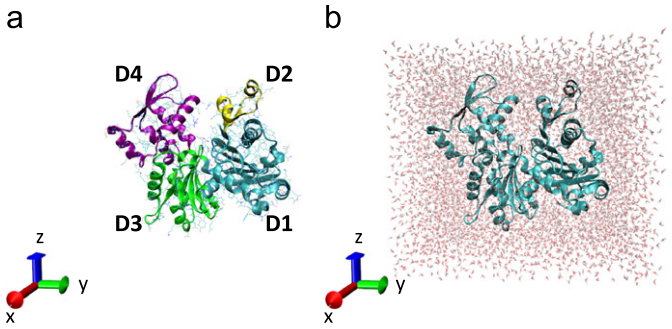

Fig. 1. Molecular models of G-actin. (a) G-actin consists of four subdomains, labelled with numbers from D1 to D4: subdomain D1 (blue) includes residues 1–32, 70–144, 338–372; subdomain D2 (yellow) is formed by residues 33–69; subdomain D3 (green) includes residues 145–180 and 270–337; subdomain D4 (pink) is formed by residues 181–269. (b) G-actin solvated in a rectangular box: the protein is represented in ribbon configuration; the solvent is represented with red beads for the oxygen molecules and white beads for the hydrogens. Bonds among the solvent molecules are represented with straight lines.

Table 1
Summary of the mechanical properties of actin filaments as reported from both experimental and computational studies.

Flexural rigidity, k_f	1.9×10^{-26}–12.6×10^{-26} Nm^2
Young's modulus, Y	1.8–2.6 GPa
Persistence length, l_p	6–20 μm

broad use of Coarse Grain (CG) approaches usually based on Molecular Dynamics (MD) (Chu and Voth, 2005, 2006; Pollard et al., 2000; Wriggers and Schulten, 1997b) and Normal Mode Analysis (NMA) (Atilgan et al., 2001b; ben-Avraham and Tirion, 1995; Chu and Voth, 2005, 2006; Doruker et al., 2000; Liu and Pollack, 2002) with the aim of better understanding, controlling and even predicting polimerization/depolimerization dynamics and mechanical properties of actin filaments.

Employing CG models implies a high simplification of the all-atom description, thus making higher size and time scales accessible. If the essential physics of the interesting processes is captured, CG simulations results are useful to systematically study complex biological systems (Ackbarow et al., 2007; Arkhipov et al., 2006; Bahar and Rader, 2005; Bond et al., 2007; Chang et al., 2006; Chng and Yang, 2008; Chu and Voth, 2006, 2007; Deriu et al., 2010a, 2010b; Gautieri et al., 2009; Orsi et al., 2008; Qin et al., 2010; Tozzini, 2005; Xu et al., 2010).

Nevertheless, in the case of F-actin, the phenomena at molecular scale, such as the surface interactions among actin monomers, should be considered explicitly. Indeed, F-actin is a hierarchically organized structure, where the monomer-to-monomer interactions are mainly responsible for its stability and stiffness. Other approaches, by reducing the all-atom structure of G-actin into few beads, e.g., each representing a functional subdomain (ben-Avraham and Tirion, 1995), lost completely the information about the shapes of the surfaces of contact between adjacent monomers, even if the strength of the interactions was reproduced by tuned homogenization procedures (Chu and Voth, 2006).

Summarizing, F-actin plays relevant structural and functional roles, such as cell shape maintenance, extension of cellular protrusions, binding to regulatory proteins, all of them coming with specific rearrangements of peculiar loops of the G-actin building blocks. As the relationship between the structural molecular rearrangements of specific regions of G-actin and the overall mechanical behaviour of F-actin have not been truly understood yet, this study is aimed at bridging this gap. For this reason, a CG model of F-actin, able to maintain a detailed molecular description of the monomer-to-monomer contact surfaces, has been employed for a systematic analysis of F-actin mechanical properties. The investigation has been carried out by adopting a computational multi-level approach, combining MD simulations and NMA, which provides a direct link between molecular phenomena and macroscopic properties.

MD simulations allowed to refine and optimize the conformations of the G-actin monomers and their packing into F-actin, while NMA was conducted to investigate the vibrational modes of motion of F-actin by using the elastic network model (ENM) approach.

On the basis of the identified bending and stretching modes, the F-actin mechanical properties were estimated.

The model developed in this study provides (i) a description of a significant fragment of F-actin; and (ii) a realistic evaluation of the F-actin macroscopic mechanical properties, obtained by considering the entire number of residues at the molecular level, as well as the interaction surfaces between and within monomers at the mesoscale level.

2. Methods

The atomic structure of G-actin, i.e., the building block of F-actin, was taken from RCSB Protein Data Bank—PDB entry 1ATN.pdb (Kabsch et al., 1990). G-actin was arranged in a rectangular box of about $6 \times 5 \times 7$ nm^3 and was fully solvated by using the Single Point Charge explicit water model (Berendsen et al., 1984) neutralized by sodium ions (Fig. 1b). The resulting system included about 26 000 atoms (about 4000 for the protein and 22,000 for the solvent). Periodic boundary conditions were applied to the system and the energy was minimized by means of 200 steps of Steepest Descent (Hess et al., 2008; van der Spoel et al., 2005). An equilibrium MD simulation was carried out in a NVT canonical ensemble (i.e., with a constant number N of atoms, constant volume V and constant temperature T) at 300 K for 40 ns, using the force-field GROMOS 53a6, recommended for simulations of biomolecules in explicit water (Oostenbrink et al., 2005, 2004) and implemented in the code GROMACS 4 (van der Spoel et al., 2005). A detailed explanation of the GROMOS force field can be found in the supplementary material.

PROCHECK (Laskowski et al., 1996b), and VMD packages were employed for analyzing the Ramachandran plot (Laskowski et al., 1996a) and MD trajectories (Wriggers and Schulten, 1997a), respectively.

The outcome of the atomistic simulations, i.e., G-actin with its atomic coordinates renewed from the fluctuations at equilibrium (Fig. 2a), was used for the assembly of the actin filaments. In particular, the correct monomer orientation into the actin filament was achieved by docking the first G-actin on a validated structure of F-actin (PDB entry 3B5U.pdb (Cong et al., 2008)). Then, further G-actins were added longitudinally, each one rotated at 166° and translated of 2.75 nm (Chu and Voth, 2005; Holmes et al., 1990). Several models of F-actin were built (Fig. 2b and c), with lengths from 50 nm (roughly 6000 aminoacids, or alpha carbons C_α) to 500 nm (about 68,000 C_α).

A first level of coarse grain (CG) was attained as follows: an Elastic Network Model (ENM) (Atilgan et al., 2001b; Chennubhotla et al., 2005; Yang and Chng, 2008)

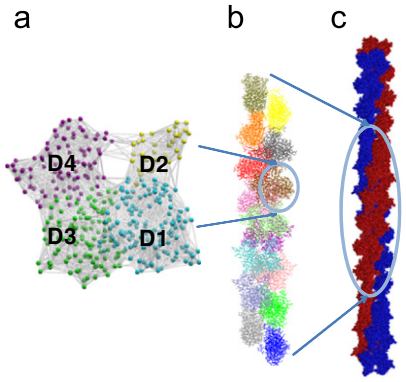

Fig. 2. (a) G-actin with its coordinates renewed from fluctuations at equilibrium: this structure is used for the built of the ENM, where the C_α represent the nodes (points) of the model and are connected to the other C_α if closer than 1.2 nm (grey bars)—C_α are clustered into rigid blocks, corresponding to the functional subdomains of G-actin (represented with different colours); (b) G-actin rotates around and translate along the filament axis, forming the architectural spiral of F-actin; and (c) the global structure of F-actin resembles that of a double helix.

was built to reduce the atomic structure of each filament in an elastic network composed of nodes (points with a mass) and springs (harmonic potentials). The nodes were set in the positions of the alpha-carbons, C_α, (Fig. 2a) and were connected by harmonic springs of 1 kcal/mol A^2 (Atilgan et al., 2001b), if closer than a cut-off distance of 1.2 nm. The total potential energy, E_p, was expressed in the anisotropic network model formulation (Doruker et al., 2000) as follows:

$$E_p = \Delta \mathbf{R}^T \mathbf{H} \Delta \mathbf{R} \quad (1)$$

where $\Delta\mathbf{R}$ is a $3N$ dimensional vector describing the fluctuations $\Delta\mathbf{R}_i$ of the position vector $\boldsymbol{R}_i$ with respect to the equilibrium position ($1 \leq i \leq N$, where N is the total number of nodes), and $\mathbf{H}$ is the Hessian matrix ($3N \times 3N$).

Owing to the large number of C_α involved (up to 68,000), the computation of the normal modes by direct diagonalization of $\boldsymbol{H}$ was not affordable. For this reason, a second level of CG was applied to the model: for every G-actin, the C_α corresponding to a functional subdomain (Fig. 1a) were clustered into a rigid block (Fig. 2a). The deformations of F-actin were expressed in terms of rotations and translations of these rigid blocks (Tama et al., 2000), adopting a Rotation Translation Block (RTB) normal mode approach (Philippe Durand et al., 1994; Tama et al., 2000). More exhaustive details on the RTB method can be found in the supplementary materials.

Assuming that F-actin behaves as an elastic rod (Kojima et al., 1994; Tsuda et al., 1996; Yasuda et al., 1996), the first modes of bending, stretching and torsion were directly related to bending stiffness (k_f), stretching stiffness (k_s) and torsional stiffness (k_t) (Bahar and Rader, 2005). Exhaustive details and the main formulas used to derive the mechanical properties from the normal modes of F-actin are given in the supplementary materials.

The contribution of the MD refinement of G-actin in determining the mechanical properties of F-actin was estimated by implementing a second model of F-actin, called the no-MD model. In the no-MD model, G-actin was not refined by carrying out preliminary MD simulations, but was taken directly from crystallography (PDB entry 1ATN.pdb (Kabsch et al., 1990)).

The mechanical properties of F-actin estimated for the two models were compared in order to identify how the topological changes reflect on the biomechanics of the filament.

3. Results

G-actin, in terms of tertiary and secondary structure, resulted stable in aqueous environment (no major unfolding took place during the MD simulation), reaching the equilibrium at about 20 ns (Fig. 3a). The root mean square deviation (RMSD) at equilibrium was around 0.4 nm (Fig. 3a). The analysis of the root mean square fluctuations (RMSF) of G-actin around its equilibrium position highlighted five peaks (Fig. 3b), with values of RMSF between 0.3 and 0.5 nm: two peaks pertained to subdomain 2 (residues 38–52 and 61–65) and three to subdomain 4 (residues 200–208, 223–230 and 241–247) (Fig. 3c). At equilibrium, the Ramachandran plot of G-actin (Fig. 3d), that displays the pairs of angles (ψ, ϕ) accessible to the structure in physiological conditions (i.e., the two degrees of backbone freedom coming from the relative rotation of two linked aminoacids around the plane of the peptide bond), highlighted that 80.1% of residues were set in the most favoured regions, while 19% and 0.3% of residues were located in additional allowed and generously allowed regions, respectively. Only a 0.6% of residues pertained to disallowed region.

The results of NMA are summarized in Table 2. It is worth noting that: the 7th mode always corresponded to the first bending mode, while the first modes of stretching and torsion were found at higher frequencies. The first mode of stretching (torsion) was found at the 15th (11st) and 29th (21st) mode for the shortest and longest F-actin, respectively. The lowest frequencies ranged from roughly 0.02 (0.03) cm^{-1} in the case of bending mode, up to about 1.21 (1.38)–0.57 (0.63) cm^{-1} for the modes of stretching and torsion in the MD (no-MD) model.

The computed values of k_f, k_s, and k_t showed to be length free. The average values of elastic stiffness's obtained from the MD model at different lengths were: $k_f = 1.22 \pm 0.09 \times 10^{-26}$ Nm^2; $k_s = 5.48 \pm 3.39\ 10^{-2}$ Nm^{-1}; and $k_t = 2.61 \pm 0.05 \times 10^{-27}$ Nm^2. Concerning with the no-MD model, the following averaged values were found: $k_f = 1.66 \pm 0.12 \times 10^{-26}$ Nm^2; $k_s = 7.03 \pm 4.2 \times 10^{-2}$ Nm^{-1}; $k_t = 3.24 \pm 0.05 \times 10^{-27}$ Nm^2. A detailed list of the values of elastic stiffness is reported in Table 3. The no-MD models

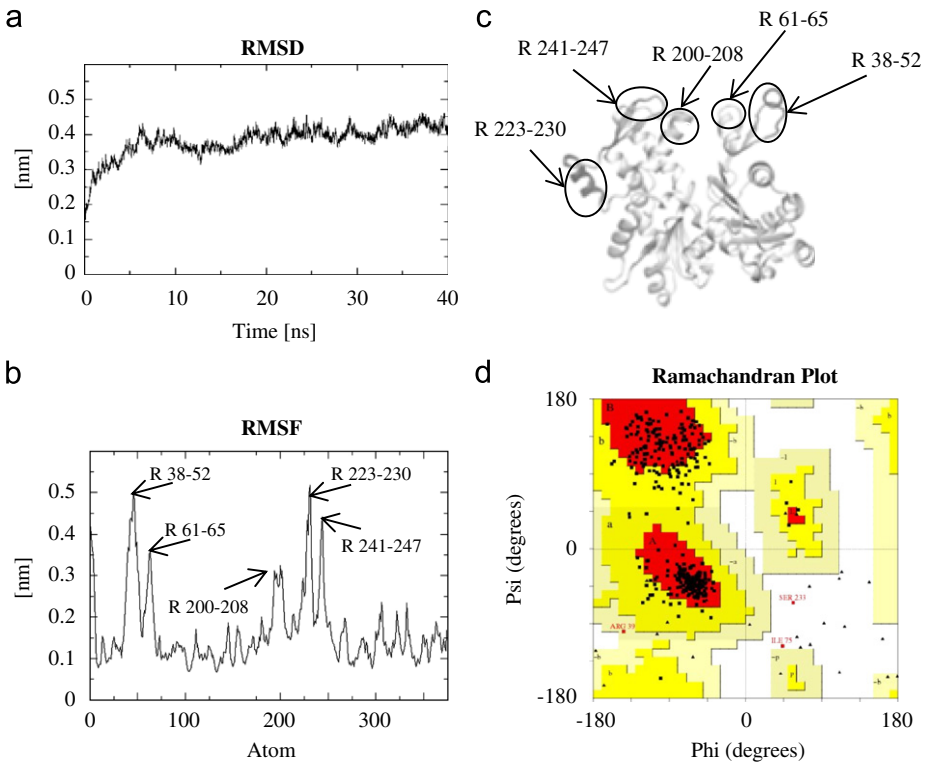

Fig. 3. (a) Root mean square deviation (RMSD) of the filament after least square fit to the protein; (b) root mean square fluctuations (RMSF) of the 375 residues of G-actin, calculated from 20 to 40 ns of equilibrium MD simulations; (c) five regions of G-actin undergoing the highest fluctuations: residues 38–52, 61–65, 200–208, 223–230 and 241–247; and (d) the Ramachandran plot: residues are indicated with black squares and triangles; red zones represent the most favoured regions; dark yellow zones and light yellow zones indicate additional and generous allowed regions, respectively; the remaining white part of the graph represents the not allowed regions.

Table 2
Mode numbers and frequencies corresponding to the 1st modes of bending, stretching and torsion as functions of different lengths of F-actin assembled after equilibrium MD, the MD model, and of F-actin assembled directly from crystallized G-actin, the no-MD model.

L [nm]	**Frequencies of MD model**						**Frequencies of no-MD model**					
	Bending		Stretching		Torsion		Bending		Stretching		Torsion	
	Mode,	f_z (cm^{-1})	Mode,	f_z (cm^{-1})	Mode,	f_z (cm^{-1})	Mode,	f_z (cm^{-1})	Mode,	f_z (cm^{-1})	Mode,	f_z (cm^{-1})
60	7	1.39	15	9.98	11	4.71	7	1.64	15	11.3	11	5.25
80	7	0.84	17	7.60	11	3.57	7	0.92	20	8.35	11	3.84
100	7	0.56	17	6.13	12	2.88	7	0.65	17	6.96	12	3.23
120	7	0.37	19	5.03	13	2.36	7	0.44	19	5.71	13	2.62
140	7	0.29	19	4.42	13	2.07	7	0.34	19	5.02	13	2.31
160	7	0.22	20	3.82	14	1.79	7	0.25	20	4.33	12	1.99
180	7	0.17	21	3.35	15	1.57	7	0.19	21	3.81	15	1.75
200	7	1.33	21	2.98	15	1.40	7	0.16	22	3.49	15	1.60
300	7	0.06	25	2.01	17	0.94	7	0.07	25	2.28	17	1.05
400	7	0.03	27	1.51	19	0.71	7	0.04	27	1.72	19	0.79
500	7	0.02	29	1.21	21	0.57	7	0.03	29	1.38	21	0.63

Table 3
Elastic stiffness's from 1st bending, stretching and torsional modes as functions of the different filament lengths for F-actin assembled after MD simulations of G-actin and build up directly from crystallized G-actin.

L (nm)	**Elastic stiffness of MD model**			**Elastic stiffness of no-MD model**		
	Bending k_f (10^{-26} Nm^2)	Stretching k_s (10^{-2} Nm^{-1})	Torsion k_t (10^{-27} Nm^2)	Bending k_f (10^{-26} Nm^2)	Stretching k_s (10^{-2} Nm^{-1})	Torsion k_t(10^{-27} Nm^2)
60	1.04	12.4	2.60	1.44	16.0	3.23
80	1.22	9.83	2.72	1.46	11.9	3.13
100	1.24	7.66	2.65	1.69	9.90	3.32
120	1.19	6.31	2.60	1.61	8.13	3.22
140	1.29	5.53	2.66	1.75	7.15	3.31
160	1.24	4.79	2.62	1.68	6.17	3.24
180	1.20	4.20	2.60	1.63	5.42	3.24
200	1.14	3.64	2.49	1.73	4.97	3.28
300	1.22	2.52	2.59	1.66	3.25	3.22
400	1.28	1.90	2.60	1.73	2.45	3.23
500	1.38	1.52	2.61	1.83	1.97	3.26

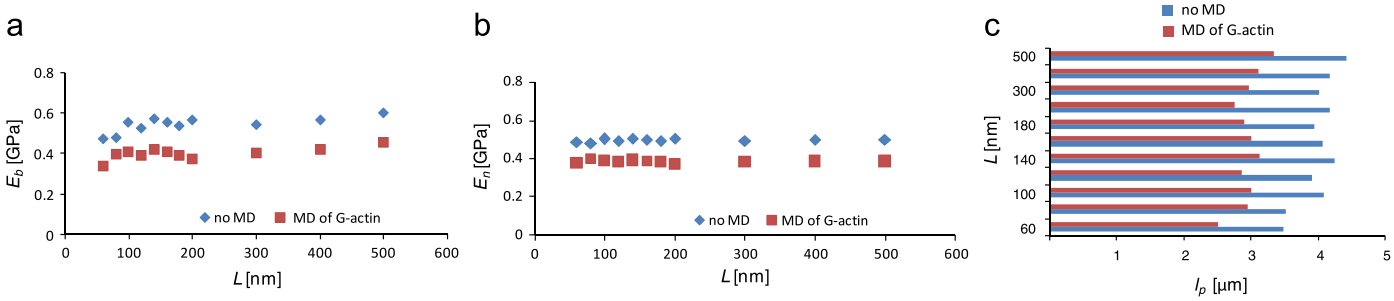

Fig. 4. (a) Bending modulus, E_b, estimated from the first mode of bending, as a function of the F-actin length, L; (b) normal modulus, E_n, computed from the first mode of stretching, as a function of L; (c) persistence length, l_p,with respect to L. The values calculated from the structures of F-actin assembled using directly the crystallographic monomer are indicated as no-MD model — black dots in (a) and (b) and black bars in (c); the values referring to F-actin assembled after MD simulation on G-actin is labelled with MD model—grey dots in (a) and (b) and grey bars in (c).

resulted always stiffer than the MD-models (Fig. 4). This fact suggests that the positions of the residues of G-actin at the output of MD simulations have an influence on the F-actin mechanical properties, that depend upon which, and how many, residue pairs interact. Indeed, the topological changes of G-actin modify the overall ENM and the vibrational modes of motion of F-actin.

The calculated bending modulus E_b resulted to be independent from the chain length, with a value of about 0.4 GPa (Fig. 4a), roughly the same value of the stretching modulus, i.e., the Young modulus, E_n, (Fig. 4b) while persistence length was about 3 μm (Fig. 4c).

4. Discussion

In comparison to the presented model, previous models of F-actin, as the one of Chu and co-workers (Chu and Voth, 2006) reduced the surfaces of interaction among subdomains: each G-actin was grained into four beads (corresponding to the four subdomains), neglecting the thousands of Å^2 of contact area among adjacent subdomains. Although employing force constants computed by a tuned approach called "fluctuation matching method" (Chu and Voth, 2006), shearing among adjacent subdomains could not be taken into account for. In our opinion, the inability of the

model of Chu and co-workers (Chu and Voth, 2006) to take into account for shearing among adjacent subdomains affected the mechanics of F-actin, particularly in terms of bending and torsional stiffness's. Indeed, Chu et al. (Chu and Voth, 2006) stated that a large cut-off (of about 20 nm) was needed to reproduce the values of persistence length computed from MD simulations on a short F-actin filament (13 monomers). On the contrary, our model took into account for shearing among adjacent subdomains and employed the standard cut-off of 1.2 nm (Atilgan et al., 2001b), estimating mechanical properties for F-actin in the same range of experimental values (Table 1).

At a second CG level, our model expressed the dynamics of F-actin as a combination of rotations and translations of the four rigid blocks of every G-actin.

In comparison with other models of F-actin (ben-Avraham and Tirion, 1995), where all G-actins were modelled as rigid units, our model did not strongly reduce the total degrees of freedom of F-actin, making a step further into the mechanical characterization of the filament. Moreover, the maximum frequencies of vibration of our models (about 0.1×10^{-12} Hz) resulted smaller than the ones (about 0.7×10^{-12} Hz) computed by ben-Avraham and Tirion (1995) as a consequence of the higher number of degrees of freedom of our model.

With reference to the local changes of G-actin, the instability of residues 30–52 (Fig. 3b and c), that form the DNase-I binding loop, can be ascribed to the high flexibility of this loop (Tirion et al., 1995), subjected to a conformational transition during actin polymerization (Chu and Voth, 2005; Oda et al., 2009; Otterbein et al., 2001). Previous studies (Oda et al., 2009) suggested that when G-actin is assembled into F-actin, the DNase-I binding loop becomes enveloped in a hydrophobic plug of the subsequent monomer on the same strand, thus confirming the tendency, here observed, for this region to move away from the polar solvent.

Moreover, the instability of residues 61–65, 200–208, 223–230 and 241–247 (Fig. 3b and c) was caused by a continuous rearrangement of the hydrophobic lateral residues, since these regions are involved in monomer-to-monomer contacts. In detail, when G-actin is assembled into F-actin, residues 61–65, 200–208 and 241–247 move to the vicinity of the neighbouring monomer of the same strand (Oda et al., 2009). Similarly, residues 223–230 interact with Cys-374 of the near monomer of the opposing strand, strengthening diagonal contacts between G-actins (Tirion et al., 1995). However, since Cys-374 presented a RMS fluctuation value lower than that of residues 223–230 (Fig. 3b), the binding between two adjacent lateral monomers in this area should be driven only by fluctuations of residues 223–230.

Interestingly, all these highly fluctuating residues are involved in interactions with nearby monomers in the double helical configuration (Oda et al., 2009): the highest fluctuations were observed for (i) four groups of residues involved in molecular interactions with the nearby monomers on the same strand, e.g., the DNase-I binding loop playing a role in the maintenance of longitudinal interactions; and (ii) one region (residues 223–230) forming diagonal contacts with the near monomer on the opposite strand, thus affecting lateral interactions. In particular, a conformational rearrangement of the DNase-I binding loops is able to weaken or stiffness the filament. Depending on its orientation, the DNase-I binding loops reduces or increases the contact surface toward the adjacent monomer on the same strand. F-actin stiffness is also affected by orientation and displacements of the hydrophobic plug, depending on the portion of exposed surface to the neighbour monomer on the opposite strand.

The most unstable regions of G-actin are those involved in contacts with nearby monomers of the same strand, indicating lower interactions between monomers of opposite strands (in other words, the longitudinal interactions among monomers are stronger than lateral ones). This fact is confirmed by the computed torsional rigidity, that resulted lower than flexural rigidity of one order of magnitude and consistent with experimental studies (Gittes et al., 1993; Isambert et al., 1995; Ott et al., 1993; Yanagida et al., 1984).

The computed persistence length l_p of F-actin resulted in the same order of magnitude of the values reported in Table 1 (Chu and Voth, 2006; Isambert et al., 1995; Janmey et al., 1994; Tsuda et al., 1996; Yang and Chng, 2008). In comparison with other cytoskeleton filaments, l_p of F-actin resulted roughly three orders of magnitude smaller than l_p of microtubules (Deriu et al., 2010a, 2010b; Gittes et al., 1993).

The applied RTB approach, based on reducing the degrees of freedom of the entire structure by defining group of particles as rigid domains, makes the F-actin stiffer than it is in reality. Nevertheless, it should be noticed that our CG model was based on the functional subdivision of the G-actin monomer (four subdomains), already experimentally identified (Kabsch et al., 1990) and used as a CG strategy in previous computational works.

Sensitivity analyses on our CG actin model, showed that increasing the number of blocks from 4 (which means 93 residues for rigid blocks) to 25 (which means 15 residues per rigid block) leads to a decrease of 30% of the bending frequency, still within the range of experimental data. Enhancing the number of blocks would allow subdomain rearrangements, during filament deformation, but it would limit the characterization of actin filaments with lengths comparable with the ones found in cells (of hundreds of nm).

Concluding, our CG model is based on two main assumptions (i.e., two coarse grain levels). At a first CG level, the orientation-dependent properties of aminoacids, as those giving rise to specific hydrogen bond pairing to stabilize alpha helix or beta sheets, were neglected and the model could not integrate the steric effects. On the other hand this method has been demonstrated to be able to reproduce the main features of protein dynamics in previous studies (Atilgan et al., 2001a; Bahar et al., 1997; Deriu et al., 2010b; Doruker et al., 2000; Hinsen, 1998). At a second CG level, internal flexibilities of the G-actin subdomains were lost, thus their contribution in determining F-actin normal modes was not taken into account.

In future developments, strategies for different block divisions should be considered, for example on the basis of the analysis of collective modes starting from the data obtained by MD simulations or NMA on single G-actin monomers. This would enhance the comprehension about the molecular rearrangements of identified subdomains during F-actin deformation.

Furthermore a proper refinement of G-actin within F-actin, for example by means of MD simulations, could be addressed, by means of equilibrium MD simulations, in order to explicitly reproduce the molecular contacts and to investigate their consequences on the global behaviour of F-actin. In addition, coordinates of the entire curved filaments (e.g., atomic trajectories obtained as outcome of NMA) could be used as input parameters for further all-atoms or coarse grain MD investigations aimed at evaluating the conformational changes and interactions of G-actin in the not deformed and deformed region of the actin filaments.

Concluding, a first contribution of this work to the study of the mechanical properties of F-actin relies on the elucidation of the characteristics of actin flexibility on the basis of the intermonomer interactions in the assemblies. It is worth noting that the computational multi-level model of F-actin here used was built only with geometrical information and with the functional form of the force field, without introducing any experimental parameter regarding the mechanics of a single monomer, e.g., the stiffness of G-actin. The results obtained are in agreement with previous findings and gave us the possibility to get insights into the biomechanics of F-actin starting from a molecular level of description.

Therefore, our work provides a link between atomistic and continuum scales modelling, describing the macroscale mechanics of actin filaments as a result of localized nanoscale phenomena.

In light of these findings, it is possible to simulate and predict the effects of specific local changes on the mechanics of F-actin owing to pathological conditions (e.g., single point mutations), or therapeutic treatments such as the effects of bound pharmacological molecules, and their consequences on the overall properties of the filament. Moreover, this progress in understanding protein materials using a bottom-up approach could further contribute to the evolutionary design of biological materials, whose properties at different scales are determined by several nanoscopic features.

Conflict of interest statement

None

Appendix A. Supplementary Materials

Supplementary data associated with this article can be found in the online version at doi:10.1016/j.jbiomech.2010.11.014.

References

Ackbarow, T., Chen, X., Keten, S., Buehler, M.J., 2007. Hierarchies, multiple energy barriers, and robustness govern the fracture mechanics of alpha-helical and beta-sheet protein domains. Proc. Natl. Acad. Sci. USA 104, 16410–16415.

Arkhipov, A., Freddolino, P.L., Imada, K., Namba, K., Schulten, K., 2006. Coarse-grained molecular dynamics simulations of a rotating bacterial flagellum. Biophys. J. 91, 4589–4597.

Atilgan, A.R., Durell, S.R., Jernigan, R.L., Demirel, M.C., Keskin, O., Bahar, I., 2001a. Anisotropy of fluctuation dynamics of proteins with an elastic network model. Biophys. J. 80, 505–515.

Atilgan, A.R., Durell, S.R., Jernigan, R.L., Demirel, M.C., Keskin, O., Bahar, I., 2001b. Anisotropy of fluctuation dynamics of proteins with an elastic network model. Biophys. J. 80, 505–515.

Bahar, I., Atilgan, A.R., Erman, B., 1997. Direct evaluation of thermal fluctuations in proteins using a single-parameter harmonic potential. Fold Des. 2, 173–181.

Bahar, I., Rader, A.J., 2005. Coarse-grained normal mode analysis in structural biology. Curr. Opin. Struct. Biol. 15, 586–592.

ben-Avraham, D., Tirion, M.M., 1995. Dynamic and elastic properties of F-actin: a normal-modes analysis. Biophys. J. 68, 1231–1245.

Berendsen, H.J.C., Postma, J.P.M., Vangunsteren, W.F., Dinola, A., Haak, J.R., 1984. Molecular-dynamics with coupling to an external bath. J. Chem. Phys. 81 (3684–3690).

Bond, P.J., Holyoake, J., Ivetac, A., Khalid, S., Sansom, M.S., 2007. Coarse-grained molecular dynamics simulations of membrane proteins and peptides. J. Struct. Biol. 157, 593–605.

Cameron, L.A., Svitkina, T.M., Vignjevic, D., Theriot, J.A., Borisy, G.G., 2001. Dendritic organization of actin comet tails. Curr. Biol. 11, 130–135.

Chang, C.E., Shen, T., Trylska, J., Tozzini, V., McCammon, J.A., 2006. Gated binding of ligands to HIV-1 protease: Brownian dynamics simulations in a coarse-grained model. Biophys. J. 90, 3880–3885.

Chennubhotla, C., Rader, A.J., Yang, L.W., Bahar, I., 2005. Elastic network models for understanding biomolecular machinery: from enzymes to supramolecular assemblies. Phys. Biol. 2, S173–S180.

Chng, C.-P., Yang, L.-W., 2008. Coarse-grained models reveal functional dynamics – II. molecular dynamics simulation at the coarse-grained level – theories and biological applications. Bioinform. Biol. Insights 2008.

Chu, J.W., Izveko, S., Voth, G.A., 2006. The multiscale challenge for biomolecular systems: coarse-grained modeling. Mol. Simulation 32, 211–218.

Chu, J.W., Voth, G.A., 2005. Allostery of actin filaments: molecular dynamics simulations and coarse-grained analysis. Proc. Natl. Acad. Sci. USA 102, 13111–13116.

Chu, J.W., Voth, G.A., 2006. Coarse-grained modeling of the actin filament derived from atomistic-scale simulations. Biophys. J. 90, 1572–1582.

Chu, J.W., Voth, G.A., 2007. Coarse-grained free energy functions for studying protein conformational changes: a double-well network model. Biophys. J. 93, 3860–3871.

Cong, Y., Topf, M., Sali, A., Matsudaira, P., Dougherty, M., Chiu, W., Schmid, M.F., 2008. Crystallographic conformers of actin in a biologically active bundle of filaments. J. Mol. Biol. 375, 331–336.

Deriu, M.A., Soncini, M., Bidone, T., Redaelli, A., Montevecchi, F.M., 2010a. Coarse Grain Modeling for Microtubule Mechanics. Mater. Sci. Forum 638–642, 629–634.

Deriu, M.A., Soncini, M., Orsi, M., Patel, M., Essex, J.W., Montevecchi, F.M., Redaelli, A., 2010b. Anisotropic elastic network modeling of entire microtubules. Biophys. J. 99 (7), 2190–2199.

Doruker, P., Atilgan, A.R., Bahar, I., 2000. Dynamics of proteins predicted by molecular dynamics simulations and analytical approaches: application to alpha-amylase inhibitor. Proteins 40, 512–524.

Fujime, S., Ishiwata, S., 1971. Dynamic study of F-actin by quasielastic scattering of laser light. J. Mol. Biol. 62, 251–265.

Gardel, M.L., Valentine, M.T., Crocker, J.C., Bausch, A.R., Weitz, D.A., 2003. Microrheology of entangled F-actin solutions. Phys. Rev. Lett. 91, 158302.

Gautieri, A., Uzel, S., Vesentini, S., Redaelli, A., Buehler, M.J., 2009. Molecular and mesoscale mechanisms of osteogenesis imperfecta disease in collagen fibrils. Biophys. J. 97, 857–865.

Gittes, F., Mickey, B., Nettleton, J., Howard, J., 1993. Flexural rigidity of microtubules and actin filaments measured from thermal fluctuations in shape. J. Cell Biol. 120, 923–934.

Gov, N.S., Gopinathan, A., 2006. Dynamics of membranes driven by actin polymerization. Biophys. J. 90, 454–469.

Hess, B., Kutzner, C., van der Spoel, D., Lindahl, E., 2008. GROMACS 4: algorithms for highly efficient, load-balanced, and scalable molecular simulation. J. Chem. Theory. Comput. 4, 435–447.

Hinsen, K., 1998. Analysis of domain motions by approximate normal mode calculations. Proteins 33, 417–429.

Holmes, K.C., Popp, D., Gebhard, W., Kabsch, W., 1990. Atomic model of the actin filament. Nature 347, 44–49.

Howard, J., 2001. Mechanics of Motor Proteins and The Cyto-Skeleton. Sinauer, Sunderland, pp. 119–134.

Isambert, H., Venier, P., Maggs, A.C., Fattoum, A., Kassab, R., Pantaloni, D., Carlier, M.F., 1995. Flexibility of actin filaments derived from thermal fluctuations. effect of bound nucleotide, phalloidin, and muscle regulatory proteins. J. Biol. Chem. 270, 11437–11444.

Janmey, P.A., Hvidt, S., Kas, J., Lerche, D., Maggs, A., Sackmann, E., Schliwa, M., Stossel, T.P., 1994. The mechanical properties of actin gels. elastic modulus and filament motions. J. Biol. Chem. 269, 32503–32513.

Jeon, J., Alexander, N., Weaver, A., Cummings, P., 2008. Protrusion of a virtual model lamellipodium by actin polymerization: a coarse-grained langevin dynamics model. J. Stat. Phys. 133, 79–100.

Kabsch, W., Mannherz, H.G., Suck, D., Pai, E.F., Holmes, K.C., 1990. Atomic structure of the actin:DNase I complex. Nature 347, 37–44.

Kabsch, W., Vandekerckhove, J., 1992. Structure and function of actin. Annu. Rev. Biophys. Biomol. Struct. 21, 49–76.

Kojima, H., Ishijima, A., Yanagida, T., 1994. Direct measurement of stiffness of single actin filaments with and without tropomyosin by in vitro nanomanipulation. Proc. Natl. Acad. Sci. USA 91, 12962–12966.

Laskowski, R.A., Rullmann, J.A.C., MacArthur, M.W., Kaptein, R., Thornton, J.M., 1996a. AQUA and PROCHECK-NMR: programs for checking the quality of protein structures solved by NMR. J. Biomol. NMR. 8, 477–486.

Laskowski, R.A., Rullmannn, J.A., MacArthur, M.W., Kaptein, R., Thornton, J.M., 1996b. AQUA and PROCHECK-NMR: programs for checking the quality of protein structures solved by NMR. J. Biomol. NMR 8, 477–486.

Liu, X., Pollack, G.H., 2002. Mechanics of F-actin characterized with microfabricated cantilevers. Biophys. J. 83, 2705–2715.

Lyman, E., Pfaendtner, J., Voth, G.A., 2008. Systematic multiscale parameterization of heterogeneous elastic network models of proteins. Biophys. J. 95, 4183–4192.

McCullough, B.R., Blanchoin, L., Martiel, J.L., De la Cruz, E.M., 2008. Cofilin increases the bending flexibility of actin filaments: implications for severing and cell mechanics. J. Mol. Biol. 381, 550–558.

Oda, T., Iwasa, M., Aihara, T., Maeda, Y., Narita, A., 2009. The nature of the globular- to fibrous-actin transition. Nature 457, 441–445.

Oostenbrink, C., Soares, T.A., van der Vegt, N.F., van Gunsteren, W.F., 2005. Validation of the 53A6 GROMOS force field. Eur. Biophys. J. 34, 273–284.

Oostenbrink, C., Villa, A., Mark, A.E., van Gunsteren, W.F., 2004. A biomolecular force field based on the free enthalpy of hydration and solvation: the GROMOS force-field parameter sets 53A5 and 53A6. J. Comput. Chem. 25, 1656–1676.

Orsi, M., Haubertin, D.Y., Sanderson, W.E., Essex, J.W., 2008. A quantitative coarse-grain model for lipid bilayers. J. Phys. Chem. B 112, 802–815.

Ott, A., Magnasco, M., Simon, A., Libchaber, A., 1993. Measurement of the persistence length of polymerized actin using fluorescence microscopy. Phys. Rev. E State Phys. Plasmas. Fluids Relat. Interdiscip. Top. 48, R1642–R1645.

Otterbein, L.R., Graceffa, P., Dominguez, R., 2001. The crystal structure of uncomplexed actin in the ADP state. Science 293, 708–711.

Panke, O., Cherepanov, D.A., Gumbiowski, K., Engelbrecht, S., Junge, W., 2001. Viscoelastic dynamics of actin filaments coupled to rotary F-ATPase: angular torque profile of the enzyme. Biophys. J. 81, 1220–1233.

Pfaendtner, J., Lyman, E., Pollard, T.D., Voth, G.A., 2010. Structure and dynamics of the actin filament. J. Mol. Biol. 396, 252–263.

Durand, Philippe, Trinquier, Georges, Sanejouand, Yves-Henri, 1994. A new approach for determining low-frequency normal modes in macromolecules. Biopolymers 34, 759–771.

Pollard, T.D., Blanchoin, L., Mullins, R.D., 2000. Molecular mechanisms controlling actin filament dynamics in nonmuscle cells. Annu. Rev. Biophys. Biomol. Struct. 29, 545–576.

Qin, Z., Buehler, M.J., Kreplak, L., 2010. A multi-scale approach to understand the mechanobiology of intermediate filaments. J. Biomech. 43, 15–22.

Scharf, R.E., Newman, J., 1995. Mg- and Ca-actin filaments appear virtually identical in steady-state as determined by dynamic light scattering. Biochim. Biophys. Acta 1253, 129–132.

Stricker, J., Falzone, T., Gardel, M.L., 2010. Mechanics of the F-actin cytoskeleton. J. Biomech. 43, 9–14.

Tama, F., Gadea, F.X., Marques, O., Sanejouand, Y.H., 2000. Building-block approach for determining low-frequency normal modes of macromolecules. Proteins 41, 1–7.
Tirion, M.M., ben-Avraham, D., Lorenz, M., Holmes, K.C., 1995. Normal modes as refinement parameters for the F-actin model. Biophys. J. 68, 5–12.
Tozzini, V., 2005. Coarse-grained models for proteins. Curr. Opin. Struct. Biol. 15, 144–150.
Tsuda, Y., Yasutake, H., Ishijima, A., Yanagida, T., 1996. Torsional rigidity of single actin filaments and actin-actin bond breaking force under torsion measured directly by in vitro micromanipulation. Proc. Natl. Acad. Sci. USA 93, 12937–12942.
van der Spoel, D., Lindahl, E., Hess, B., Groenhof, G., Mark, A.E., Berendsen, H.J., 2005. GROMACS: fast, flexible, and free. J. Comput. Chem. 26, 1701–1718.
Wriggers, W., Schulten, K., 1997a. Protein domain movements: detection of rigid domains and visualization of hinges in comparisons of atomic coordinates. Proteins 29, 1–14.
Wriggers, W., Schulten, K., 1997b. Stability and dynamics of G-actin: back-door water diffusion and behavior of a subdomain 3/4 loop. Biophys. J. 73, 624–639.
Xu, Z., Paparcone, R., Buehler, M.J., 2010. Alzheimer's abeta(1–40) amyloid fibrils feature size-dependent mechanical properties. Biophys. J. 98, 2053–2062.
Yanagida, T., Nakase, M., Nishiyama, K., Oosawa, F., 1984. Direct observation of motion of single F-actin filaments in the presence of myosin. Nature 307, 58–60.
Yang, L.W., Chng, C.P., 2008. Coarse-grained models reveal functional dynamics–I. Elastic network models–theories, comparisons and perspectives. Bioinform. Biol. Insights 2, 25–45.
Yasuda, R., Miyata, H., Kinosita Jr., K., 1996. Direct measurement of the torsional rigidity of single actin filaments. J. Mol. Biol. 263, 227–236.